
Mechanisms of separation of rupture area and variation in time interval and size of great earthquakes along the Nankai Trough, southwest Japan

Takane Hori

*Institute for Research on Earth Evolution, Japan Agency for Marine-Earth Science and Technology
3173-25 Showa-machi, Kanazawa-ku, Yokohama 236-0001, Japan
E-mail: horit@jamstec.go.jp*

(Received January 20, 2006; Revised manuscript accepted March 2, 2006)

Abstract According to the earthquake history along the Nankai Trough more than 1000 years, two great inter-plate earthquakes have occurred east and west off Kii Peninsula within a few years and such earthquakes have occurred repeatedly with 100-200 years intervals. Recent seismic structure surveys along the Nankai Trough reveal that there are some heterogeneous structures in several tens of kilometer scale at the boundaries of the separated rupture areas. For example, high velocity and high density doming body exists beneath Kii Peninsula, which is the main segmentation boundary. We consider that such large-scale heterogeneous structures may control the rupture area separation. The heterogeneity should be also related to the mechanism of variation in time interval and size of great earthquakes occurred there, because such mechanism is closely related how rupture propagation stops. To investigate the mechanisms of rupture area separation and also time- and size-variation of great earthquakes along the Nankai Trough, we conducted large-scale numerical simulation of earthquake generation cycles. Heterogeneous distribution in frictional properties is assumed based on the heterogeneous structures obtained by seismic surveys. The results show that rupture area separation can be reproduced within the reasonable range in frictional parameters. The significant variation in recurrence time and earthquake size occurs only when large fracture energy area exists in the deeper portion of the seismogenic zone. The existence of such area causes heterogeneous stress distribution after one earthquake cycle. The variation pattern obtained here is similar to that of the last three earthquake cycles in the historical data.

Keywords: Earthquake, earthquake cycle, subduction, Nankai Trough, rupture

1. Introduction

Great earthquakes, whose magnitude (M) is equal to or more than 8.0, have repeatedly occurred along the southern coast of southwest Japan, where Philippine Sea plate is subducting beneath it from the Nankai Trough (e.g. [1]). The history of earthquake generation cycles can be traced back to more than 1000 years ago [2]. A typical earthquake occurrence pattern here is that two great earthquakes occur one after another within a few years while recurrence intervals are 100-200 years (Fig. 1). The recurrence interval and size have changed somewhat systematically in recent cycles. In 1707, the largest earthquake (moment magnitude : $M_w = 8.7$) occurred in Tokai (C + D + E) and Nankai (A + B) areas almost simultaneously [3, 4]. About 150 years after that, Tokai (C + D + E, $M_w = 8.4$) and Nankai (A + B, $M_w = 8.5$) earthquakes occurred separately with 32 hours interval in 1854 [3,4]. The latest events occurred in 1944 (Tonankai: C + D, $M_w = 8.2$, [5]) and 1946 (Nankai: A + B, $M_w = 8.4$, [6]). The recurrence intervals and earthquake sizes become smaller in time while the time intervals

between Tokai (C + D + E) or Tonankai (C + D) and Nankai (A + B) earthquakes become longer.

For both the 1944 Tonankai and 1946 Nankai earthquakes, rupture started from off Kii Peninsula and propagated unilaterally in the east and west, respectively [7] (Fig. 2). The rupture areas of the two events are not overlapped and there is no large gap between them [8]. The eastern part of the rupture area of the 1944 Tonankai earthquake does not include off Tokai area, where the rupture propagated in the 1854 Tokai earthquake (Fig. 1). These suggest that at least two barriers for the rupture propagation exist at the eastern and western boundaries of the 1944 Tonankai rupture area. Recent seismic structure surveys reveal that significant structure heterogeneities, such as subducting ridge and seamounts with diameter of around 50 km, exist at the boundaries [e.g. 9]. We examine here if such heterogeneous structures can control the rupture propagation using numerical simulation of earthquake generation cycles along the Nankai Trough.

In previous simulation studies, separated rupture areas were modeled as separated blocks [e.g. 10, 11]. Such

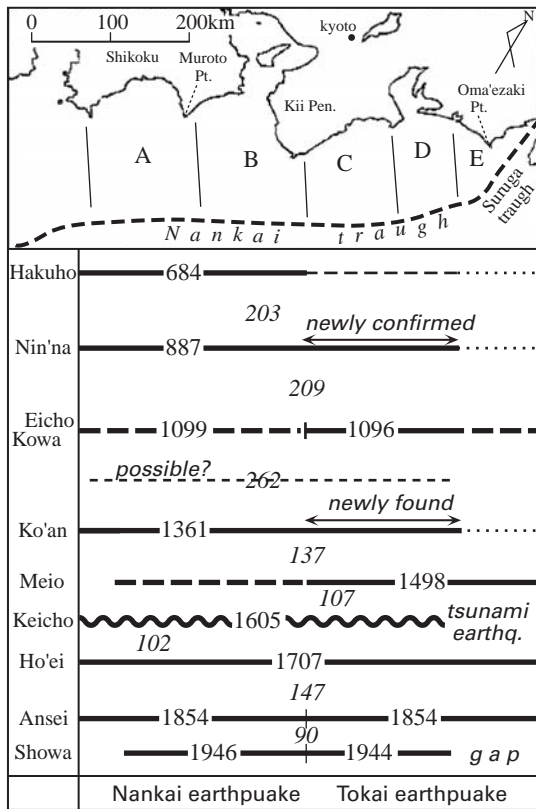


Fig. 1 Space-time distribution of great earthquakes along the Nankai-Suruga trough (after [2]). Roman and italic numerals indicate earthquake occurrence years and time intervals between two successive series, respectively. Thick solid, thick broken, and thin broken lines show certain, probable, and possible rupture zones, respectively. Thin dotted lines mean unknown.

models, of course, cannot examine how the rupture areas are separated. In order to examine the effect of the heterogeneous structures with their spatial extent, it is necessary to model the plate boundary not as separated blocks but as a continuum fault plane. Hori et al. [12] constructed a model of earthquake generation cycles on a large fault plane of 691 km × 307.2 km, which represents a subducting Philippine Sea plate beneath southwest Japan from Tokai to Shikoku. In their model, depth variation in frictional properties is included. Although heterogeneity in frictional property related to the large-scale (~100 km) variation of plate geometry is included as depth variation of frictional parameters, rupture propagates through the whole area in every earthquake cycle. In this paper, we introduce smaller scale (~50 km) heterogeneity in frictional property based on the results of structure surveys and examine whether rupture area separation can be reproduced or not. Moreover, the mechanism for the variation in recurrence interval and earthquake size is also investigated.

2. Modeling procedures

2.1 Basic equations

Earthquake cycles are modeled as repetition of stick and slip on an area along the plate boundary. The stick area is loaded by the velocity difference between the stick area and its outside where stable sliding with plate convergence rate occurs. For simplicity, the slip direction is fixed in our model. Only one component of the shear

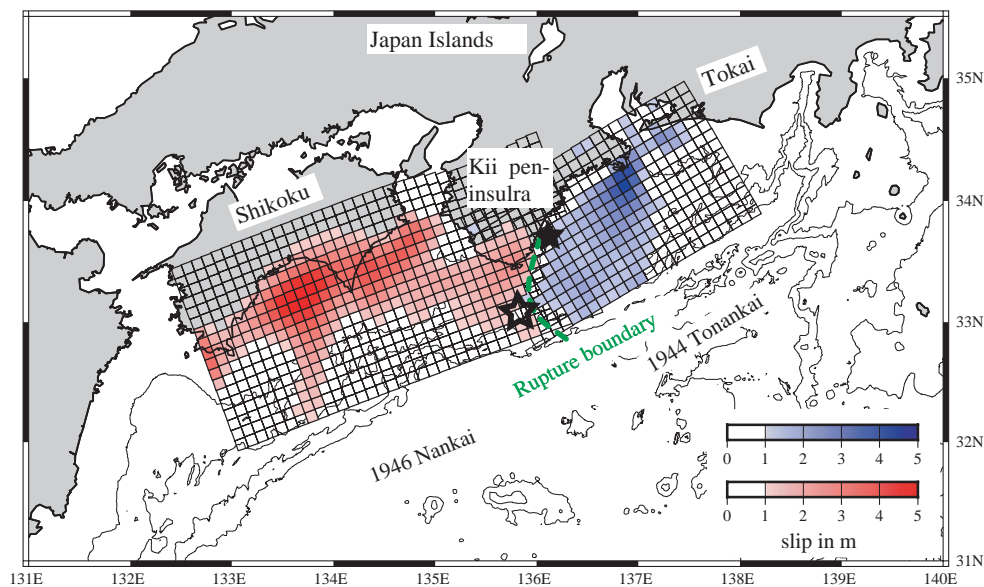


Fig. 2 Slip distributions of the 1944 Tonankai and 1946 Nankai events estimated by using small subfaults (10 km × 10 km) with the smoothness constrain: Blue and red scales show the amount of slip on the subfaults during the respective events (modified from [8]). Solid and open stars indicate epicenters of the Tonankai and Nankai events, respectively [7]. The boundary between the rupture areas of the earthquakes were clearly imaged (green dot curve).

traction on the plate boundary, which is parallel to the slip direction, is considered here. The shear stress at a point on the plate boundary is expressed as follows.

$$\tau(r, t) = \int K(r; r') \{ \delta(r', t) - V_{pl}(r') t \} dr' - \frac{G}{2\beta} V(r, t), \quad (1)$$

where τ , δ , V and V_{pl} are the shear stress, the slip, the slip velocity and the plate convergence rate, respectively. $(\delta - V_{pl}t)$ represents the slip deficit relative to the plate convergence rate. $K(r; r')$ is the static shear stress change at r caused by a unit dislocation at r' . Since K does not include dynamic stress changes, the second term is necessary to represent the dumping factor for energy radiation through seismic waves [13].

It is controlled by frictional properties whether an area is stick-slip one or stable sliding one. A friction law used here, so called rate- and state-dependent friction law, is derived from laboratory experiments [e.g. 14, 15]. Given the shear stress τ , the slip velocity V and the state variable Θ , which determines the frictional strength [16], change according to the equations below.

$$\tau(r, t) = \sigma(r) \left[\mu_* + \Theta(r, t) - a(r) \ln \left\{ \frac{V_*}{V(r, t)} + \frac{V_*}{V_{st}} \right\} \right], \quad (2)$$

$$\begin{aligned} \frac{d\Theta(r, t)}{dt} &= \frac{b(r) V_*}{L(r)} \exp \left[-\frac{\Theta(r, t)}{b(r)} \right] \exp \left[\frac{V(r, t)}{V_c} \right] \\ &\quad - \frac{V(r, t)}{L(r)} \left[\Theta(r, t) - b(r) \ln \left\{ \frac{V_*}{V(r, t)} + \frac{V_*}{V_{st}} \right\} \right], \end{aligned} \quad (3)$$

where σ is the effective normal stress, which is assumed to be constant, a , b and L are frictional parameters, V_* and μ_* are an arbitrarily chosen reference slip velocity and the steady-state frictional coefficient at $V = V_*$. V_* is set to be plate convergence rate V_{pl} here. V_{st} ($= 0.1 \text{ mm/s}$) represents the saturation velocity of the rate effect on steady-state friction at high slip velocities [17, 18]. V_c ($= 0.01 \text{ } \mu\text{m/s}$) is a cutoff velocity for the friction law derived by [15]. The values of a , b and L basically determine the frictional property as shown in Fig. 3. We will describe how to determine the distribution of these values in the later section (2.3).

To obtain the space-time distribution of slip velocity, we derive a differential equation for the slip velocity from equations (1) and (2).

$$\begin{aligned} \frac{dV(r, t)}{dt} &= \frac{\int K(r; r') \{ V(r; r') - V_{pl}(r') \} dr' + \sigma(r) d\Theta(r; t)/dt}{a(r) \sigma(r) / \{ 1/V(r, t) + 1/V_{st} \} + G/2\beta}. \end{aligned} \quad (4)$$

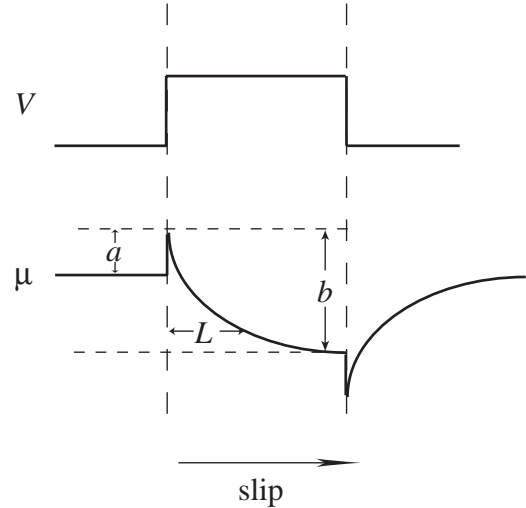


Fig. 3 Illustration of the rate effects on friction using a single-state-variable constitutive law: from top to bottom are shown the given velocity change; the resulting change in friction (modified from [39]).

The set of first-order differential equations (3) and (4) is numerically solved after spatial discretization described in the next section.

2.2 Model geometry and discretization

The subducting Philippine Sea plate is simply modeled by a flat thrust fault plane in a three dimensional homogeneous isotropic elastic half space as shown in Fig. 4. The dip angle of the plane is roughly equal to that of the subducting plate east of the Kii Peninsula [19]. The parameters of the elastic medium are listed in Table 1. The plate convergence direction is assumed to be constant and uniform in 58 degree clockwise from the x axis on the fault plane (Fig. 4a). The plate convergence rate is estimated from GPS data as shown in Fig. 4b [20]. We assumed that the convergence rate smoothly changes only in the x direction.

To represent the slip velocity distribution on the fault plane, it is discretized into 147,456 subfaults, each of which is 1.2 km by 1.2 km in the x and the y directions. The slip velocity and the state variable are uniform on each subfault. The discretized differential equations are as follows,

$$\frac{dV_i(t)}{dt} = \frac{\sum_j K_{ij} (V_j(t) - V_{pl,j}) + \sigma_i d\Theta_i(t)/dt}{a_i \sigma_i / \{ 1/V_i(t) + 1/V_{st} \} + G/2\beta}, \quad (5)$$

$$\begin{aligned} \frac{d\Theta_i(t)}{dt} &= \frac{b_i V_{pl,i}}{L_i} \exp \left[-\frac{\Theta_i(t)}{b_i} \right] \exp \left[\frac{V_i(t)}{V_c} \right] \\ &\quad - \frac{V_i(t)}{L_i} \left[\Theta_i(t) - b_i \ln \left\{ \frac{V_{pl,i}}{V_i(t)} + \frac{V_{pl,i}}{V_{st}} \right\} \right]. \end{aligned} \quad (6)$$

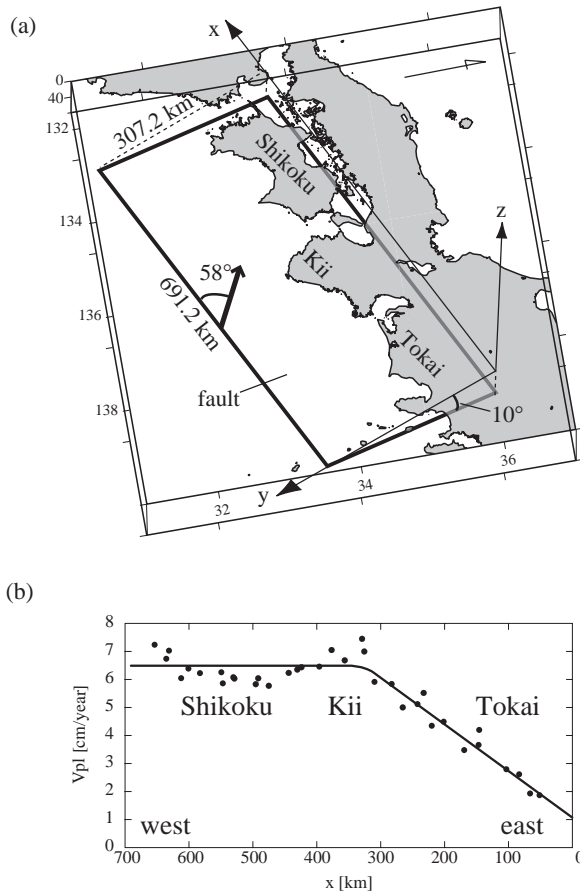


Fig. 4 (a) The coordinate system and the fault geometry used to calculate static shear stress change (after [12]). The area of the fault plane and dip of the fault are shown. The thick arrow indicates the direction of plate convergence assumed in this study [40]. (b) The dots and the solid line indicate the plate convergence rates estimated by Heki and Miyazaki [20] and those used in this study, respectively.

Table 1 Parameters of elastic medium used to calculate static shear stress K_{ij} .

Parameter	Value
rigidity	33 GPa
Poisson's ratio	0.25
density	$2.8 \times 10^3 \text{ kg/m}^3$
S-wave velocity	3.4 km/s

The shear stress is calculated at the center of each sub-faults for K_{ij} . The initial conditions are that $V_i(0) = 0.9V_{pl,i}$ and $\Theta_i(0) = -b_i \ln(V_i(0)/V_{pl,i})$. The above equations are numerically solved using the Runge-Kutta method with an adaptive step-size control [21]. The step size for time integration depends how fast velocity or state variable changes. In one earthquake cycle, step size is large ($\sim 0.1 \text{ year} = 3 \times 10^6 \text{ s}$) for interseismic period and becomes very small ($< 0.005 \text{ s}$) for coseismic period (Fig. 5).

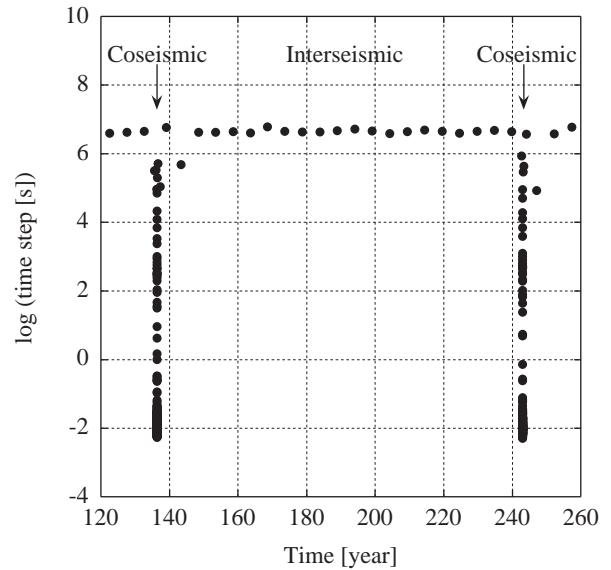


Fig. 5 An example of temporal variation in time steps for calculation of an earthquake cycle using the Runge-Kutta method with an adaptive step-size control.

We use 128 nodes (1024 processors) of the Earth Simulator with a single-level flat MPI model. To calculate 6 earthquake cycles (about 660 years), it took 7.5 hours for one case and similar time for other cases. In this case we achieved 3.6 Tflops, which is 44 % of the peak speed. The vector performance was also good (99.4%).

2.3 Distribution of frictional properties

Frictional properties depend on temperature based on laboratory experiments [22]. Since temperature distribution on the plate boundary has not been known yet, we simply assumed that frictional parameters basically depend on depth. The depth of the plate interface was mapped on the flat fault plane in our model as shown in Fig. 6a. The geometry of subducting plate was determined from hypocenter distribution of microseismicity and seismic refraction surveys [12].

The depth distribution of the frictional parameters a , b and L , and the effective normal stress σ is shown in Fig. 6. The region where $a - b$ is negative corresponds to the seismogenic zone, where stick and slip occur. The shallower and deeper limit of the zone roughly corresponds to the depth of deformable backstop [23] and the bottom depth of slow slip events along the Nankai Trough [24, 25]. The maximum value of $b - a$ ($= 0.5 \times 10^{-3}$) is determined so as to fit the average recurrence time interval (117 years) of historical earthquakes along the Nankai Trough [26]. The characteristic slip distance, L , which is a memory distance over which the contact population changes, is constant in shallower portion of the seismo-

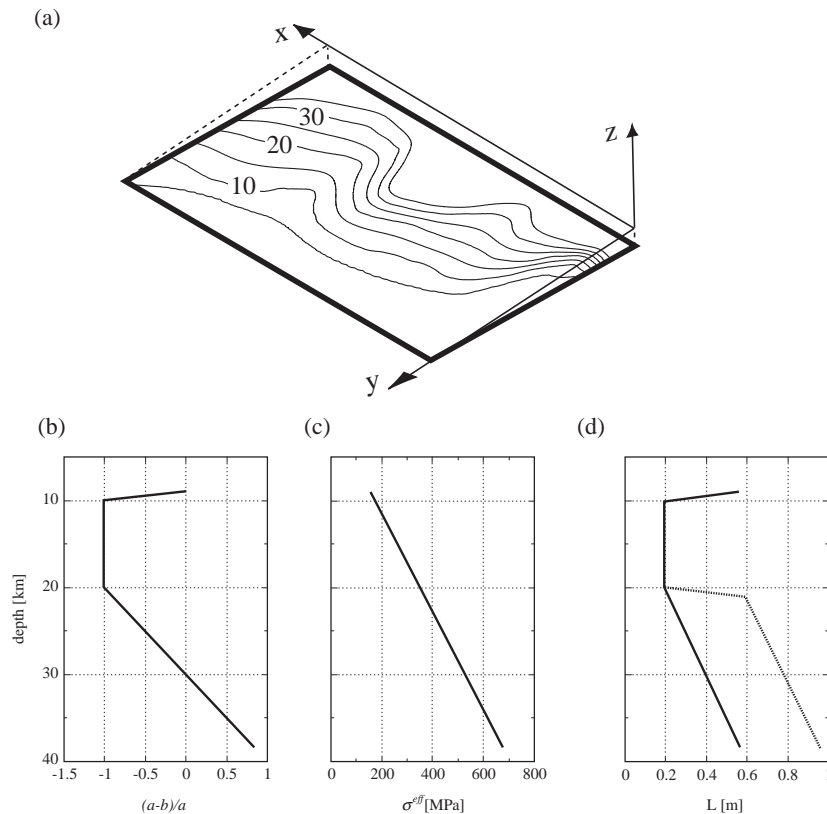


Fig. 6 (a) Contour lines with numerals indicate the depth and geometry of the slab mapped on the fault model plane. The contour interval is 5 km. (b) The depth dependence of $(a - b)/a$. (c) The depth dependence of effective normal stress σ^{eff} . (d) The depth dependence of the frictional parameter L . For deeper depth, solid line is for cases 1A and 2A. Dashed line is for cases 1B and 2B. Depth in (b), (c), and (d) is that for the slab geometry mapped on the model fault plane shown in (a).

genic zone but larger in the deeper part based on the laboratory experiment [27]. We apply two cases for depth dependence of L . One smoothly increases with depth but the other suddenly increases in the upper part of the transition zone from seismic to aseismic (Fig. 6d). The effective normal stress is given by $\sigma = (\rho - \rho_w)gz$, where ρ , ρ_w , g and z are rock density, water density, gravity acceleration and depth. The former three values are $2.8 \times 10^3 \text{ kg/m}^3$, $1.0 \times 10^3 \text{ kg/m}^3$ and 9.8 m/s^2 , respectively. We refer the case with depth dependent frictional properties as case 1. Cases 1A and 1B correspond to the cases with smoothly increase in L and suddenly increase in L , respectively.

Other than the depth dependence of frictional properties above, we introduce here heterogeneous frictional properties based on structural heterogeneity such as a subducting seamount [9]. Recent dense structural surveys along the Nankai Trough reveal that there are significant heterogeneities in seismic structures in the rupture segmentation boundaries [9, 28, 29]. Off Tokai and Shikoku, ridges and seamounts, whose diameter is several tens of km, are subducting beneath the upper crust. An effect of

subducted topographic high is estimated to be at most 200 MPa increase in normal stress [30]. So we applied the additional normal stress (max. 200 MPa) off Tokai and Shikoku. At another rupture segmentation boundary off Kii Peninsula, a high velocity doming body was found just above the plate boundary [29]. This anomaly may cause additional load (~ 30 MPa) on the plate boundary by the density contrast and several times higher $(b - a)$ value than those of the surrounding sedimentary rocks based on laboratory experiments [31]. The product of these two factors provides larger $(b - a)\sigma$ value, which is comparable to those at the subducted ridges or seamounts. Additionally, a fracture zone is found along the shallower part of the boundary of the 1944 Tonankai and 1946 Nankai rupture areas [29]. For this fracture zone, we introduce $b = 0$ area to represent the unlocked plate interface. In terms of the characteristic slip distance L , an area preventing propagation is expected several times larger L than the surrounding area [13]. We, therefore, apply 4.5 to 6 times larger L in those structures, depending on their sizes. We refer the case with heterogeneous frictional

properties based on structural heterogeneity as case 2. According to the depth dependence in L , we calculate two cases: cases 2A and 2B as for the cases 1A and 1B. The distribution of $(b - a) \sigma$ and L values for cases 2A and 2B is shown in Fig. 7.

3. Simulation results

3.1 Depth-dependent frictional property (cases 1A and 1B)

The earthquake cycles were solved for depth-dependent frictional properties. In this case, an identical earthquake occurs repeatedly with almost constant time interval. For different depth-dependence of L (cases 1A and 1B), recurrence time interval is 109.5 ± 0.0 years and 110.6 ± 0.2 years, respectively. Fig. 8 shows calculated slip velocity distribution during one example of earthquake cycles for case 1A. Low and high velocity areas (blue and orange colored areas in Fig. 8) can be regarded

as stick and seismic slip areas, respectively. Wide white areas represent stable sliding area with plate convergence rate. In the interseismic period, most of the seismogenic zone is stick and stress is accumulated there (Fig. 8a). The stick area becomes narrower in the later stage of the interseismic period (Fig. 8b). Just before the occurrence of seismic slip, slow slip occurs off Kii Peninsula (Fig. 8c). The slip is accelerated to seismic slip velocity and propagates bilaterally to east and west (Figs. 8d-f). After the seismic slip reaches to the both ends of fault plane, slip velocity decreases and after slip occurs mainly in the deeper part and its extent of the seismogenic zone (Fig. 8g). The distribution of coseismic slip (slip velocity is higher than 1 cm/s) for case 1A is shown in Fig. 8h. The rupture area extends from Tokai to Shikoku. The total seismic moment for this case is $1.0 \pm 0.0 \times 10^{22}$ Nm, which corresponds to the moment magnitude (M_w) of 8.6.

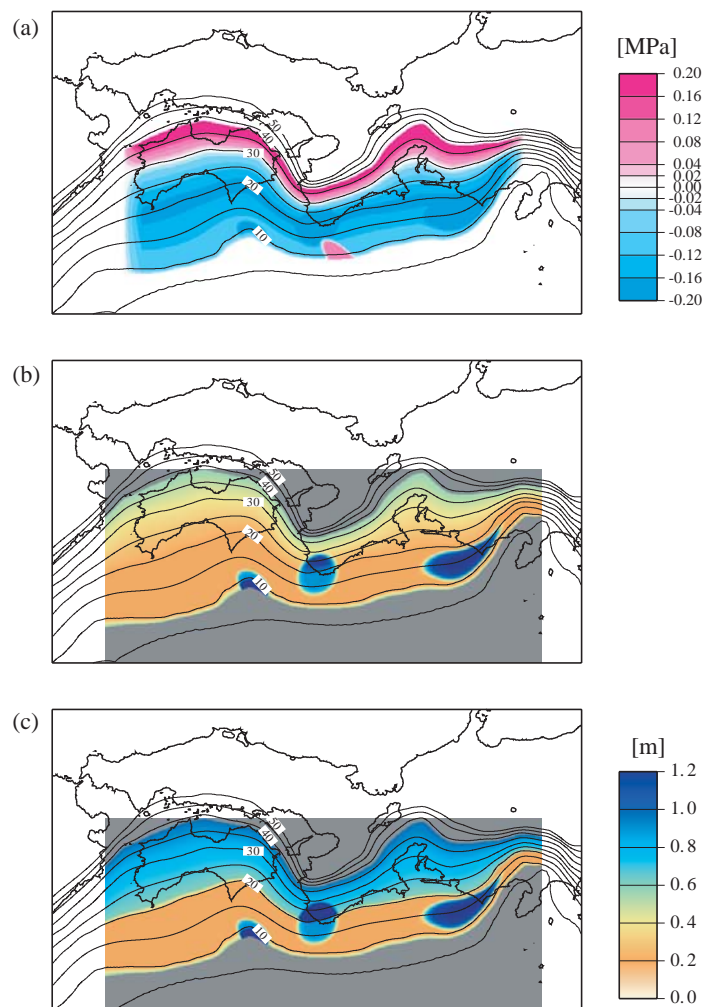


Fig. 7 (a) The value of $(a - b) \sigma$ at each cell is plotted for case 2. The contour shows the isodepth lines of the slab geometry. (b) The value of L for case 2A. (c) The value of L for case 2B.

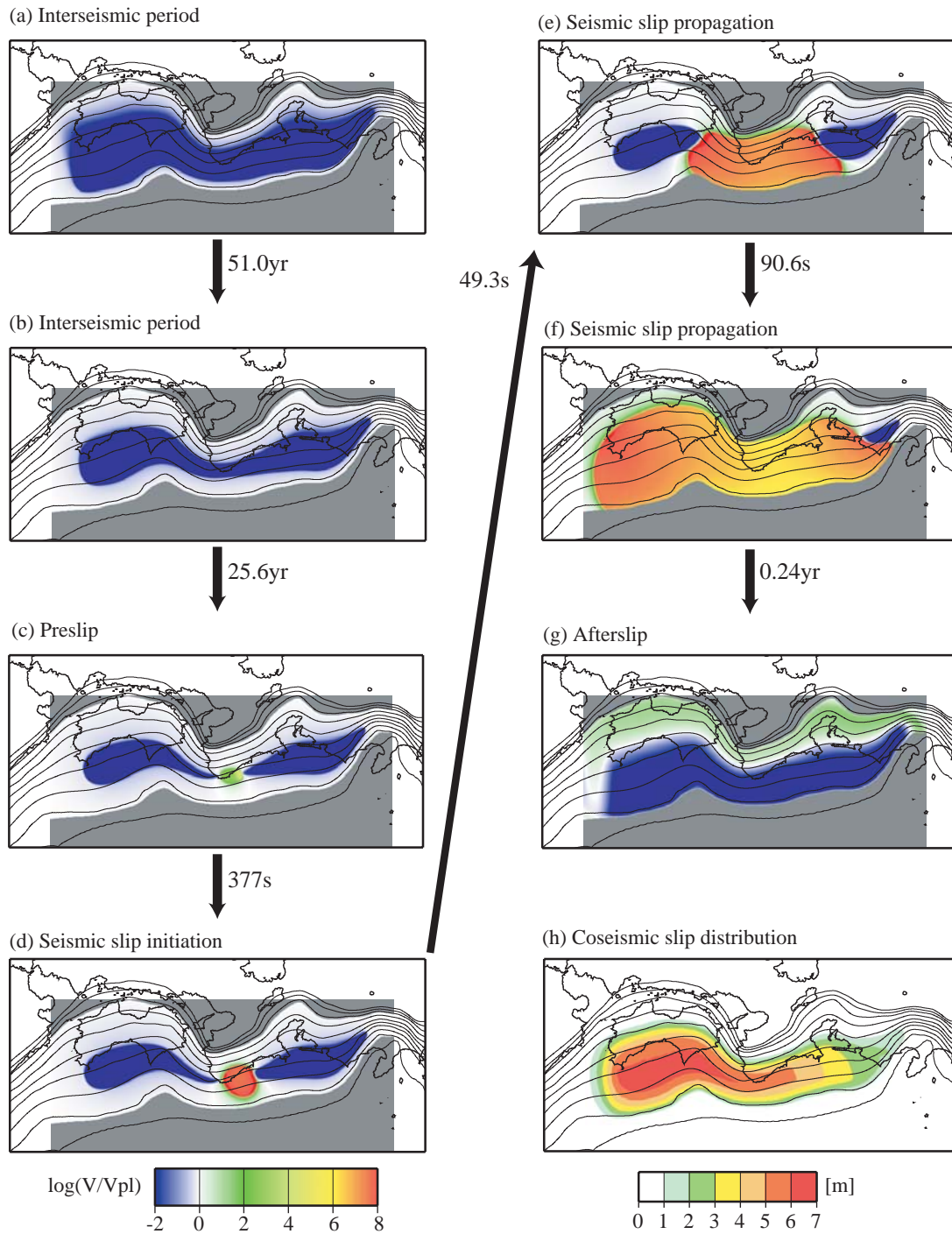


Fig. 8 (a-g) Snapshots of the slip velocity distribution normalized to the plate convergence rate for case 1A. Blue and red indicate locking and unstably slipping parts of the fault, respectively. Each numeral and time unit accompanied by an arrow shows the time interval between two snapshots. (h) Distribution of coseismic slip (slip velocity higher than 1 cm/s).

3.2 Heterogeneous frictional properties related to structural anomalies (case 2A)

Rupture area separation can be reproduced if we introduce heterogeneous frictional properties based on the major structural anomalies such as subducted ridges. All the coseismic slip patterns of the events are shown in Fig. 9. These patterns repeat cyclically. Tonankai event

starts from the western edge (off Kii Peninsula) and rupture propagates to the east. Once in two earthquake cycles, the rupture propagates into the Tokai segment (Fig. 9a). After a few or several days, Nankai event starts from the eastern edge (off Kii Peninsula) and propagates to the west (Figs. 9b, d). The time interval between Tonankai and Nankai events is 4.3 ± 2.3 days for 5 pairs. Recurrence

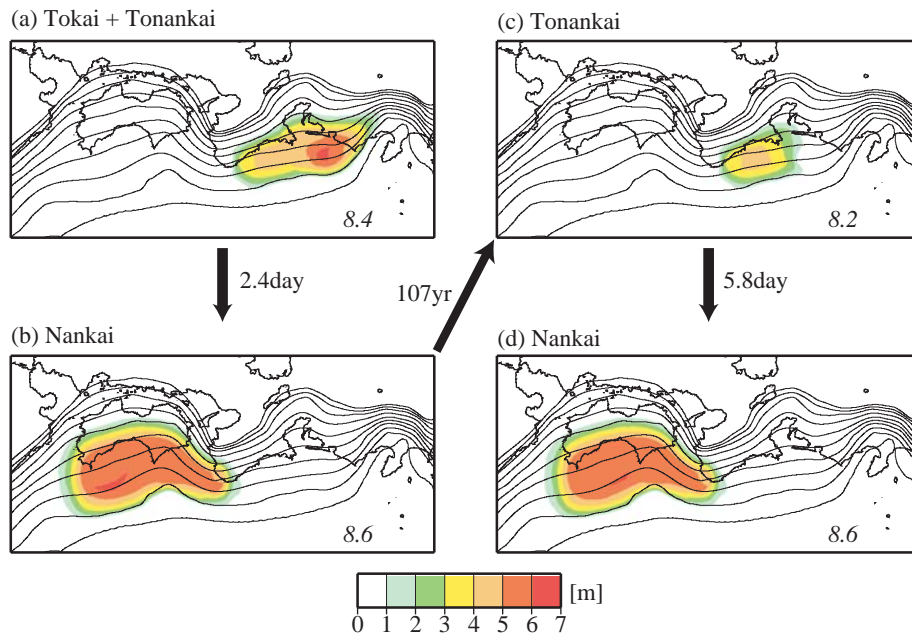


Fig. 9 Distribution of coseismic slip (slip velocity higher than 1 cm/s) for case 2A. Each numeral and time unit accompanied by an arrow shows the time interval between two earthquakes. Italic numerals indicate the moment magnitude. All the slip patterns are shown.

interval of Tonankai or Nankai event is 106.0 ± 0.8 years for 4 earthquake cycles. The variation in recurrence interval is fairly larger than that in case 1A. Seismic moment [Nm] and M_w of Tonankai, Tonankai + Tokai, Nankai events are $2.3 \pm 0.0 \times 10^{21}$ (8.2), 5.4×10^{21} (8.4) and $1.1 \pm 0.0 \times 10^{22}$ (8.6), respectively. Seismic slip always starts off Kii Peninsula as case 1.

3.3 Larger characteristic slip distance in the deep part (case 2B)

Significant variation in recurrence time of each event and time interval between Tonankai and Nankai events are seen in the results both with large characteristic slip distance L in the deep part of the seismogenic zone and with heterogeneous frictional properties based on structure surveys. All the coseismic slip patterns are shown in Fig. 10. The time interval between Tonankai and Nankai events and its variation (34.4 ± 42.0 days) are about ten times larger than those in case 2A (4.3 ± 2.3 days). Once in three earthquake cycles, the time interval becomes significantly short (one or two hours) and we plot these successive events as one earthquake in Fig. 10. The variation in recurrence interval of the Nankai events (106.7 ± 6.4 years) is also about ten times or much larger than the other cases (cases 1A, 1B and 2A: 109.5 ± 0.0 , 110.6 ± 0.2 and 106.0 ± 0.8 years). Furthermore, large variation in seismic moment can be seen for the Nankai events: $8.6 \pm 1.0 \times 10^{21}$ Nm, although no variation more than 0.1×10^{21} Nm is seen in the other cases.

Time interval between events and event sizes seem to

change systematically (Fig. 10). After the Tonankai and Nankai events whose time interval is significantly short, the time interval becomes longer (from 26 days to 76 days or from 7 days to 97 days) for the following two earthquake cycles. Recurrence interval and size of Nankai event also systematically change. Recurrence interval becomes shorter (from 111 years to 95 years or from 109 years to 103 years) in the two cycles. Seismic moment [Nm] and M_w become smaller: from 9.4×10^{21} (8.6) to 7.2×10^{21} (8.5) or from 9.4×10^{21} (8.6) to 8.5×10^{21} (8.6).

Slip histories off Kii Peninsula, Shikoku and Tokai are shown in Figs. 11a, 11b and 11c, respectively. Gradual slip acceleration before each large slip (i.e. earthquake) occurrence can be seen off Kii Peninsula (Fig. 11a), from where rupture always starts. The acceleration points are roughly on a slip accumulation curve with the plate convergence rate (the lower dotted line in Fig. 11a). Slip amount becomes smaller ($s_1 > s_2 > s_3$) and then a slow slip occurs (ss). After the slow slip, slip amount (s_4) becomes large in the next cycle. Similar slip amount variation can be seen off Shikoku (Fig. 11b). However, no gradual slip acceleration and no slow slip occur here. Additionally, not slip starting points but slip ending points are on a line with the plate convergence rate (see the upper dotted line in Fig. 11b). Significantly longer recurrence interval is found for off Tokai (Fig 11c). Slip ending points are on a line with the plate convergence rate, which is fairly lower than the other two areas.

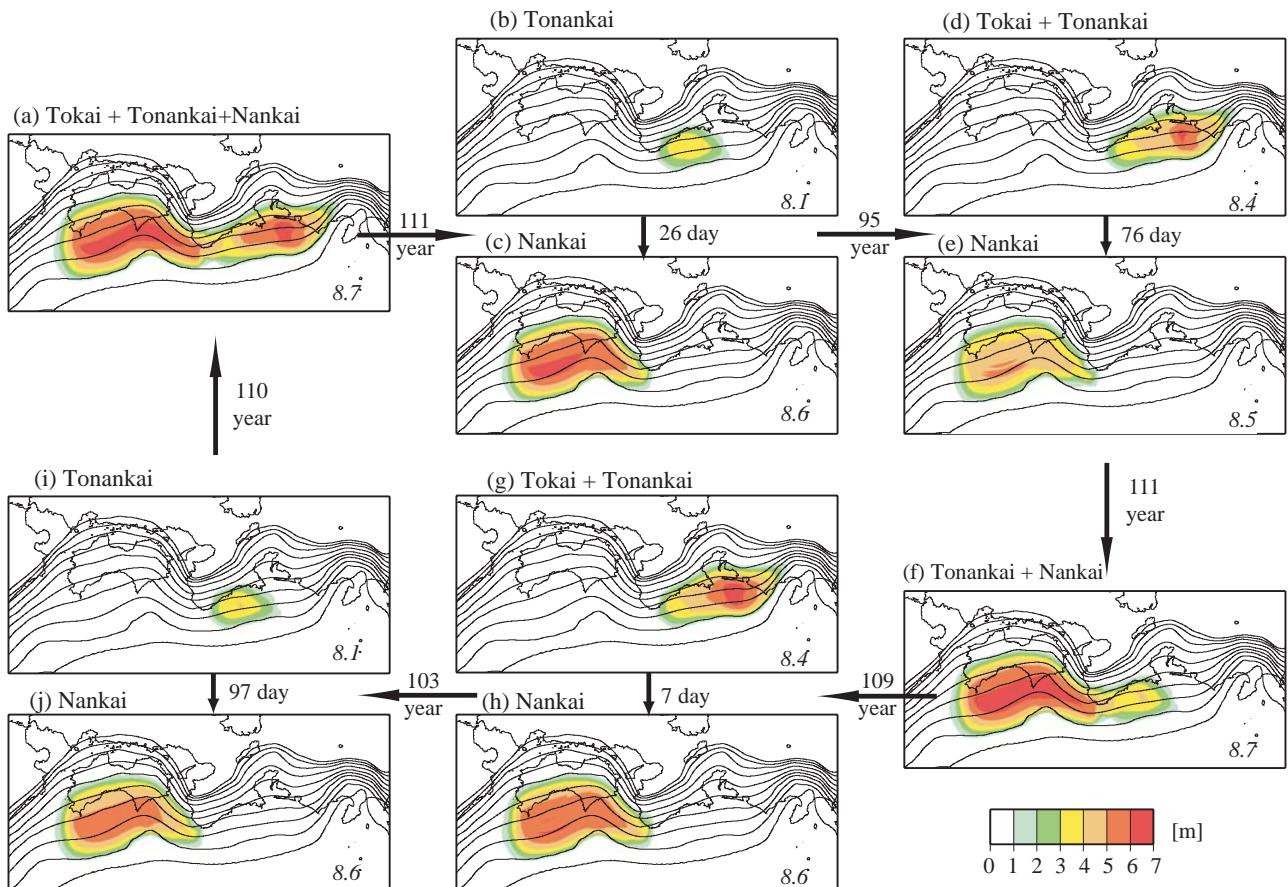


Fig. 10 Distribution of coseismic slip (slip velocity higher than 1 cm/s) for case 2B. Each numeral and time unit accompanied by an arrow shows the time interval between two earthquakes. Italic numerals indicate the moment magnitude. All the slip patterns are shown.

4. Discussion

4.1 Preseismic slip and rupture initiation off Kii Peninsula

All the results show that the preseismic slip occurs and rupture starts off Kii Peninsula. This is consistent with that both 1944 Tonankai and 1946 Nankai earthquakes initiated there, although it is difficult to know the rupture initiation points for former historical events. We discuss here how the preseismic slip occurs and rupture initiates off Kii Peninsula as shown in the simulation results. This can be explained by combining effects of a narrower seismogenic zone width due to the higher dip angle here and the lateral variation in the plate convergence rate [12]. Both affect the stress accumulation rate. The seismogenic zone is narrower, the locked zone in the interseismic period is narrower. This results in the higher stress accumulation rate [32]. Although the seismogenic zone is the narrowest off Tokai, the plate convergence rate is so low that the stressing rate cannot be high. On the other hand, the seismogenic zone off Kii Peninsula is narrower than the surrounding area (Fig. 7a) and the plate convergence rate is almost the maximum value along the Nankai Trough (Fig. 4b). Thus, the stress accumulation rate is the highest

and slip rate significantly accelerates at first off Kii Peninsula.

4.2 Variation in recurrence interval and earthquake size

The calculated variation pattern in time interval and size of earthquakes for case 2B (Fig. 10) is similar to the historical earthquakes from 1707 (Fig. 1). For both the simulation results and historical data, after the largest earthquake, the recurrence interval and earthquake size become smaller and the time intervals between Tokai (or Tonankai) and Nankai earthquakes become longer. This systematic variation can be explained as follows. The heterogeneous frictional properties based on structure (Figs. 7a and 7c) and large characteristic slip distance anomaly in the deeper part of seismogenic zone (broken line in Fig. 6d) causes smaller slip than the accumulated slip deficit in and around the barriers, where fracture energy is significantly high. Accumulated slip deficit remains after an earthquake cycle (d2 in Fig. 11a) off Kii Peninsula, that is rupture initiation point and is near one of the barriers. On the other hand, accumulated slip deficit is released completely in the main slip area far

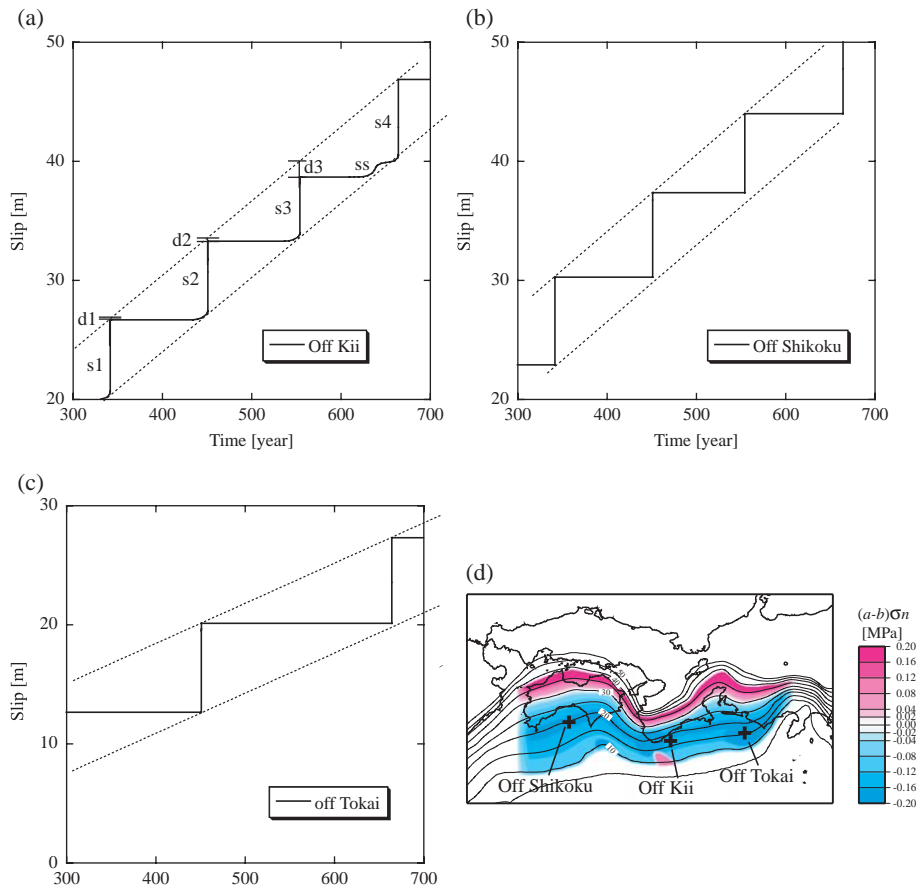


Fig. 11 Cumulative slip on the plate boundary off Kii peninsula (a), off Shikoku (b) and off Tokai (c). The positions are shown in (d). Broken lines in (a), (b) and (c) indicate plate convergence rate. See text for explanation of marks s1, d1 and so on.

from the barriers (Figs. 11b and 11c). This heterogeneous slip distribution near the barrier off Kii Peninsula causes high stress level in the rupture initiation point after the earthquake cycle and so rupture initiation timing of the following earthquake becomes earlier. The size of the following earthquake should become smaller because lower amount of slip deficit can be accumulated in the main slip area like off Shikoku during the shorter time interval (Fig. 11b). The smaller size of the earthquake results in the larger remaining in slip deficit in the rupture initiation point ($d3 > d2$ in Fig. 11a). In this way, the recurrence interval and size become smaller and smaller. The time interval between Tokai (or Tonankai) and Nankai earthquakes depends on the size of Tokai (or Tonankai) earthquake and on the recurrence time interval. If the size of Tokai (or Tonankai) event is large, stress level becomes high in the eastern end of the Nankai area. If the recurrence time interval is long, stress level in the whole Nankai area is high. Both can let Nankai earthquake occur earlier. Thus the time interval between Tokai (or Tonankai) and Nankai earthquake becomes longer if the recurrence interval and size become smaller.

4.3 Slow slip and the following large earthquake

The size of earthquake becomes smaller and finally slow slip event occur in the rupture initiation area (ss in Fig. 11a). This is because the stress level is not high enough to cause unstable slip. Although the slip velocity is low, the slow slip breaks a part of the barrier off Kii Peninsula and also makes the stress level high in the remaining part of the barrier. After the slow slip event, the stress builds up again in the rupture initiation area. During the slow slip event and the following period, slip deficit is accumulated continuously in the main slip area. When a nucleation starts again, the stress level of the barrier and the main slip area is significantly high. Thus the barrier is easily broken and the earthquake size becomes large. In this case, accumulated slip deficit is released completely in the whole rupture area.

4.4 Parameter dependence of the results

The recurrence interval of each earthquake depends both on $(b - a)\sigma$ and L [33]. So we can choose different sets of these values for the same recurrence interval. If smaller L value is chosen, the rupture starts not from off

Kii Peninsula but from western edge of the model. As shown in Figs. 8a and 8b, stable sliding area become large near the western edge because of the loading effect at the edge. This slip accelerates earlier than the slip off Kii Peninsula when smaller L value is used. In this case, rupture always propagates through the Kii Peninsula and no segmentation occurs off Kii Peninsula. On the other hand, if larger L value is chosen, slip instability becomes weak and no large seismic slip can occur [34]. Both rupture patterns for smaller and larger L values are completely different from that seen in historical data.

Whether rupture stops or not also depends both on the distribution of $(b - a) \sigma$ and L values. Their spatial pattern and the values of $(b - a) \sigma$ are determined in case 2 based on other observational or experimental information as described in 2.3. Additional examination is necessary to check if the L value used here is reasonable. As shown in [35, 36], the larger value of L causes the larger critical slip weakening distance D_c , which has a scaling relation with the seismic moment $M_0 = 10^{19} D_c^3$ [37]. From our results, D_c is about 5 - 6 m obtained in the slip-stress relation at the large L area. The seismic moment M_0 is about 3×10^{21} Nm for the Tokai area. The D_c value is comparable to that expected from the scaling relation (6.7 m). Thus we conclude that the anomaly in frictional parameters of both $(b - a) \sigma$ and L is reasonable. The validity of the distribution of frictional property given here supports that the structure heterogeneities, such as subducted ridge with the radius of several tens kilometers, are possible factors to control the extent of the rupture area as barriers for rupture propagation.

Acknowledgement

I wish to thank the researchers in Research Program for Plate Dynamics, Institute for Research on Earth Evolution (IFREE) and also the members in the collaboration project in cooperation with the Earth Simulator Center entitled "Simulation of Earthquake Generation Process in a Complex System of Faults". I also thank Prof. Yuzo Hamano for his constructive comments. The Earth Simulator was used for all the simulations. I would like to thank all members of the Earth Simulator Center for their support. The Generic Mapping tools package [38] was used for depicting the plate configuration and creating some figures.

(This article is reviewed by Dr. Yuzo Hamano.)

Reference

[1] M. Ando, Source mechanisms and tectonic significance of historical earthquakes along the Nankai trough, Japan, *Tectonophysics*, vol. **27**, pp.119–140, 1975.

[2] K. Ishibashi, Status of historical seismology in Japan, *Ann. Geophys.*, vol. **47**, pp.339–368, 2004

[3] I. Aida, Numerical experiments of historical tsunamis generated off the coast of the Tokai district, *Bull. Earthq. Res. Inst.*, vol. **56**, pp.367–390, 1981.

[4] I. Aida, Numerical experiments of historical tsunamis generated off the coast of the Nankaido district, *Bull. Earthq. Res. Inst.*, vol. **56**, pp.713–730, 1981.

[5] Y. Tanioka and K. Satake, Detailed coseismic slip distribution of the 1944 Tonankai earthquake estimated from tsunami waveforms, *Geophys. Res. Lett.*, vol. **28**, pp.1075–1078, 2001.

[6] T. Baba, Y. Tanioka, P.R. Cummins, and K. Uehira, The slip distribution of the 1946 Nankai earthquake estimated from tsunami inversion using a new plate model, *Phys. Earth Planet. Inter.*, vol. **132**, pp.59–73, 2002.

[7] H. Kanamori, Tectonic implications of the 1944 Tonankai and the 1946 Nankaido earthquakes, *Phys. Earth Planet. Inter.*, vol. **5**, pp.129–139, 1972.

[8] T. Baba and P.R. Cummins, Contiguous rupture areas of two Nankai Trough earthquakes revealed by high-resolution tsunami waveform inversion, *Geophys. Res. Lett.*, vol. **32**, L08305, doi:10.1029/2004GL022320, 2005.

[9] S. Kodaira, A. Nakanishi, J.O. Park, A. Ito, T. Tsuru, and Y. Kaneda, Cyclic ridge subduction at an inter-plate locked zone off central Japan, *Geophys. Res. Lett.*, vol. **30**, 1339, doi:10.1029/2002GL016595, 2003.

[10] J. Huang and D.L. Turcotte, Evidence for chaotic fault interactions in the seismicity of the San Andreas fault and Nankai trough, *Nature*, vol. **348**, pp.234–236, 1990.

[11] N. Mitsui and K. Hirahara, Simple spring-mass model simulation of earthquake cycle along the Nankai trough in southwest Japan, *Pure Appl. Geophys.*, vol. **161**, pp.2433–2450, 2004.

[12] T. Hori, N. Kato, K. Hirahara, T. Baba, and Y. Kaneda, A numerical simulation of earthquake cycles along the Nankai trough, southwest Japan: Lateral variation in frictional property due to the slab geometry controls the nucleation position, *Earth Planet. Sci. Lett.*, vol. **228**, pp.215–226, 2004.

[13] J. R. Rice, Spatio-temporal complexity of slip on a fault, *J. Geophys. Res.*, vol. **98**, pp.9885–9907, 1993.

[14] C. Marone, Laboratory-derived friction laws and their application to seismic faulting, *Annu. Rev. Earth Planet. Sci.*, vol. **26**, pp.643–696, 1998.

[15] N. Kato and T. E. Tullis, A composite rate- and state-dependent law for rock friction, *Geophys. Res. Lett.*, Vol. **28**, pp.1103–1106, 2001.

[16] M. Nakatani, A new mechanism of slip weakening and strength recovery of friction associated with the mechanical consolidation of gouge, *J. Geophys. Res.*, vol. **103**, pp.27239–27256, doi:10.1029/98JB02639, 1998.

- [17] S. T. Tse and J. R. Rice, Crustal earthquake instability in relation to the depth variation of frictional slip properties, *J. Geophys. Res.*, vol.**91**, pp.9452–9472, 1986.
- [18] J. H. Dieterich, Time-dependent friction and the mechanics of stick-slip, *Pure Appl. Geophys.*, vol.**116**, pp.790–806, 1978.
- [19] A. Nakanishi, N. Takahashi, J. O. Park, S. Miura, S. Kodaira, Y. Kaneda, N. Hirata, T. Iwasaki, and M. Nakamura, Crustal structure across the coseismic rupture zone of the 1944 Tonankai earthquake, the central Nankai Trough seismogenic zone, *J. Geophys. Res.*, vol.**107**, doi:10.1029/2001JB000424, 2002.
- [20] K. Heki and S. Miyazaki, Plate convergence and long-term crustal deformation in central Japan, *Geophys. Res. Lett.*, vol.**28**, pp.2313–2316, 2001.
- [21] W. H. Press, S. A. Teukolsky, W. T. Vetterling, and B. P. Flannery, *Numerical Recipes in Fortran 77: The Art of Scientific Computing*, 2nd Edition, Cambridge University Press, New York, pp.963, 1996.
- [22] M. L. Blanpied, D. A. Lockner, and J. D. Byerlee, Fault stability inferred from granite sliding experiments at hydrothermal conditions, *Geophys. Res. Lett.*, vol.**18**, pp.609–612, 1991.
- [23] A. Nakanishi, S. Kodaira, J. O. Park, and Y. Kaneda, Deformable backstop as seaward end of coseismic slip in the Nankai Trough seismogenic zone, *Earth Planet. Sci. Lett.*, vol.**203**, pp.255–263, 2002.
- [24] S. Ozawa, M. Murakami, M. Kaidzu, T. Tada, T. Sagiya, Y. Hatanaka, H. Yarai, and T. Nishimura, Detection and monitoring of ongoing aseismic slip in the Tokai region, central Japan, *Science*, vol.**298**, pp.1009–1012, 2002.
- [25] Y. Yagi and M. Kikuchi, Partitioning between seismogenic and aseismic slip as highlighted from slow slip events in Hyuga-nada, Japan, *Geophys. Res. Lett.*, vol.**30**, 1087, doi:10.1029/2002GL015664, 2003.
- [26] T. Rikitake, Recurrence of great earthquakes at subduction zones, *Tectonophysics*, vol.**35**, pp.335–362, 1976.
- [27] A. Kato, M. Ohnaka, and H. Mochizuki, Constitutive properties for the shear failure of intact granite in seismogenic environments, *J. Geophys. Res.*, vol.**108**, 2060, doi:10.1029/2001JB000791, 2003.
- [28] S. Kodaira, N. Takahashi, A. Nakanishi, S. Miura, and Y. Kaneda, Subducted seamount imaged in the rupture zone of the 1946 Nankaido Earthquake, *Science*, vol.**289**, pp.104–106, 2000.
- [29] S. Kodaira, T. Hori, A. Ito, S. Miura, G. Fujie, J. O. Park, T. Baba, H. Sakaguchi, and Y. Kaneda, A possible giant earthquake off southwestern Japan revealed from seismic imaging and numerical simulation, *J. Geophys. Res.*, 2005 (submitted).
- [30] C. H. Scholz and C. Small, The effect of seamount subduction on seismic coupling, *Geology*, vol.**25**, pp.487–490, 1997.
- [31] A. Kato, A. Sakaguchi, S. Yoshida, H. Yamaguchi, and Y. Kaneda, Permeability structure around an ancient exhumed subduction-zone fault, *Geophys. Res. Lett.*, vol.**31**, L06602, doi:10.1029/2003GL019183, 2004.
- [32] M. Matsu'ura and T. Sato, Loading mechanism and scaling relations of large interplate earthquakes, *Tectonophysics*, vol.**277**, pp.189–198, 1997.
- [33] W.D. Stuart, Forecast model for great earthquakes at the Nankai trough subduction zone, *Pure Appl. Geophys.*, vol.**126**, pp.619–641, 1988.
- [34] H. Hirose and K. Hirahara, A model for complex slip behavior on a large asperity at subduction zones, *Geophys. Res. Lett.*, vol.**29**, 2068 doi:10.1029/2002GL015825 , 2002.
- [35] M. Cocco and A. Bizzarri, On the slip-weakening behavior of rate- and state-dependent constitutive laws, *Geophys. Res. Lett.*, vol.**29**, pp.11,1–11,4, 2002.
- [36] N. Kato and T.E. Tullis, Numerical simulation of seismic cycles with a composite rate- and state-dependent friction law, *Bull. Seism. Soc. Am.*, vol.**93**, pp.841–853, 2003.
- [37] M. Ohnaka, A physical scaling relation between the size of an earthquake and its nucleation zone size, *Pure Appl. Geophys.*, vol.**157**, pp.2259–2282, 2000.
- [38] P. Wessel and W. H. F. Smith, New version of the generic mapping tools (GMT) version 3.0 released, *EOS Trans. AGU*, vol.**76**, pp.329, 1995.
- [39] C.H. Scholz, *The mechanics of earthquakes and faulting*, Cambridge Univ. Press, New York, pp .439, 1990.
- [40] S. Miyazaki and K. Heki, Crustal velocity field of southwest Japan: Subduction and arc–arc collision, *J. Geophys. Res.*, vol.**106**, pp.4305–4326, 2001.